Manuscript submitted to: Volume 2, Issue 2, 153-162.

AIMS Biophysics DOI: 10.3934/biophy.2015.2.153

Received date 02 March 2015, Accepted date 17 May 2015, Published date 21 May 2015

Research article

Decontamination of digital image sensors and assessment of electron microscope performance in a BSL-3 containment

Michael B. Sherman [1,2,3,4,*], Juan Trujillo [5], Benjamin E. Bammes [6], Liang Jin [6], Matthias W. Stumpf [7], and Scott C. Weaver [1,3,4,8]

[1] Sealy Center for Structural Biology and Molecular Biophysics, University of Texas Medical Branch, Galveston, Texas, USA
[2] Department of Biochemistry and Molecular Biology, University of Texas Medical Branch, Galveston, Texas, USA
[3] Institute for Human Infections and Immunity, University of Texas Medical Branch, Galveston, Texas, USA
[4] Center for Biodefense and Emerging Infectious Diseases, University of Texas Medical Branch, Galveston, Texas, USA
[5] JEOL USA, Inc., Peabody, Massachusetts, USA
[6] Direct Electron, LP, San Diego, California, USA
[7] E. A. Fischione Instruments, Inc., Export, Pennsylvania, USA
[8] Department of Microbiology and Immunology, University of Texas Medical Branch, Galveston, Texas, USA

* **Correspondence:** Email: mbsherma@utmb.edu; Tel: +409-392-8297.

Abstract: A unique biological safety level (BSL)-3 cryo-electron microscopy facility with a 200 keV high-end cryo-electron microscope has been commissioned at the University of Texas Medical Branch (UTMB) to study the structure of viruses and bacteria classified as select agents. We developed a microscope decontamination protocol based on chlorine dioxide gas with a continuous flow system. In this paper we report on testing digital camera sensors (both CCD and CMOS direct detector) in a BSL-3 environment, and microscope performance after chlorine dioxide (ClO_2) decontamination cycles.

Keywords: cryo-electron microscopy; single particle imaging; biological safety containment

1. Introduction

We reported previously on the development of BSL-3 containment including a high-end cryo-electron microscope to study highly pathogenic viruses and bacteria [1,2].

Studying "live" infectious agents (e.g., viruses or bacteria) presents a challenge both in the design of the facility and the logistics of its operation. Since the commissioning of the lab, several tests have been performed to prove effectiveness of chlorine dioxide (ClO_2) gas decontamination protocols, and a few agents have been studied in containment. However, until now, none of the electron detectors in the microscope has been tested for exposure to ClO_2 which could present difficulties in the containment operation if, for example, a single ClO_2 exposure during decontamination cycle would render the detectors unusable. In addition, the microscope itself could be affected by the ClO_2 treatment and its performance consequently could deteriorate significantly.

We have therefore tested two different electron detector assemblies for the cameras installed in our JEM-2200FS electron microscope (JEOL Ltd., Tokyo, Japan): a TVIPS scintillator assembly (FastScan F114T, TVIPS GmbH, Gauting, Germany) and DE-20 direct electron detector sensor module (Direct Electron, LP, San Diego, California, USA). Each of these detector assemblies was exposed to ClO_2 gas with the overall exposure dose equivalent to that of several decontamination cycles of the microscope. Their performance was tested before and after ClO_2 treatment, and the parts were examined visually.

Additionally, we used Tobacco Mosaic Virus (TMV) as a test specimen to assess performance of the microscope after multiple exposures to ClO_2. Results demonstrated safe operation of the cameras in the BSL-3 containment and a satisfactory microscope performance after exposing it to ClO_2 gas.

2. Materials and Method

2.1. Image sensors testing

Overall ClO_2 exposure cycles were implemented similar to previous reports [2], except that gas injection to and from the microscope was eliminated from the loop (Figure 1). Only the mixing chamber attached to the ClO_2 generator (Minidox M, ClorDiSys, New Jersey, USA) was included in the ClO_2 flow loop. All valves controlling the ClO_2 flow were included in the loop to provide a proper sequence of events during the decontamination cycle. A ClO_2 mixture with nitrogen at a given concentration was prepared in the mixing chamber and humidified as needed; proper concentration and humidity of the ClO_2 was measured and controlled by the ClO_2 generator during the cycle. After a decontamination cycle was complete, the system was purged with dry nitrogen gas to remove ClO_2 and residual moisture from the mixing chamber before opening the chamber to take out tested parts. ClO_2 was pushed through a neutralizing device (scrubber) during the purging stage. We used higher than usual (~1 mg/L) ClO_2 concentrations (6–10 mg/L) and longer exposure times to assess the longevity of image sensors exposed to ClO_2.

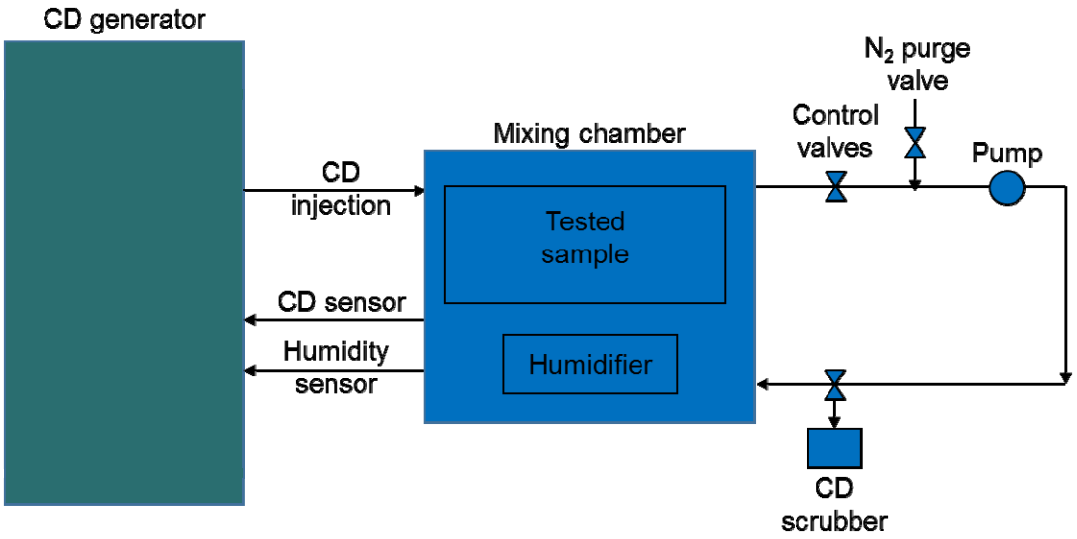

Figure 1. Schematic view of chlorine dioxide (CD, ClO_2) flow through the system. A Minidox-M generator supplied ClO_2 to the mixing chamber at the required concentration where it was humidified to facilitate the disinfection. The tested parts were enclosed in the mixing chamber. A closed loop was established between the mixing chamber and the Minidox-M, and a small diaphragm pump was used to pump the mixture through the loop. Once the required humidity level was established in the chamber and conditions stabilized, ClO_2 was injected into the mixing chamber until the required concentration was reached. ClO_2 concentration and humidity were monitored and maintained in the chamber during the cycle. After the cycle was complete, the system was purged with dry nitrogen gas and residual ClO_2 was scrubbed.

2.2. Cryo-electron microscopy

Tobacco mosaic virus (TMV) was vitrified manually as reported previously [3] on C-flat grids (Protochips, Raleigh, North Carolina). Frozen grids were stored under liquid nitrogen and transferred to a cryo-specimen 626 holder (Gatan, Inc., Pleasanton, California, USA) before loading into a JEM-2200FS electron microscope, equipped with an in-column energy filter (omega type) and a field emission gun (FEG), operating at 200 keV. Grids were maintained at near-liquid nitrogen temperature (−172 to −180 °C) during imaging. Images were acquired at 40,000× nominal microscope magnification using a DE-20 Camera System (Direct Electron, LP, San Diego, California, USA) with approximately 32 electrons/$Å^2$ total exposure; the pixel size corresponded to 1.49 Å on the specimen scale. An in-column omega electron energy filter was used during imaging with a zero-loss electron energy peak selected using a 20 eV slit. Images were collected with defocus values ranging from 0.46 to 2.0 μm.

Two datasets were acquired: first, a small set of 18 images from which 630 TMV segments (equivalent to 40,000 asymmetric units) were selected, followed by a larger set of 65 images from which ~4700 TMV segments were selected (equivalent to 300,000 asymmetric units). The camera was used in movie mode at 25 frames/s. Individual image frames for each image were aligned with

DE_process_frames.py script (Direct Electron, LP) to correct for specimen drift during image exposure and to compensate for radiation damage [4,5].

2.3. Image processing

Each dataset was processed independently using the same workflow. The processing scheme was similar to [6,7]. First, short segments were boxed from TMV particles using EMAN HELICAL BOXER program [8]; the extracted segments were CTF corrected (EMAN2 E2CTFCOR, [9]). All subsequent processing was done in IMAGIC [10]. The images were normalized and band-pass filtered between 200 and 3 Å. Segments were aligned rotationally and translationally using a vertical rectangle with soft edges as a reference and analysed by multivariate statistical analysis. The best class average was used to calculate an initial 3D reconstruction, which was helically averaged; that map was used as the initial model in projection matching MRA in IMAGIC for alignment and angular refinement. After each round of refinement by projection matching, the resulting 3D map was averaged using TMV helical parameters (49 CP subunits in 3 turns, with a height of 69 Å, a helical rise per subunit of 1.408 Å, and a rotation per subunit of 22.04° [11,12]. The effective resolution of the final maps was calculated using Fourier Shell Correlation between the smaller and larger data sets. It was estimated by the "gold-standard" criterion [13] to be 6.3 Å.

The 3D maps were surface-rendered and displayed with a one standard deviation (1σ) threshold in CHIMERA [14], which accounted for ~100% particle volume. We performed rigid body fitting of the TMV structure (2XEA.pdb [6]) into our cryo-EM density map in CHIMERA [14].

3. Results and Discussion

3.1. Using a ClO_2 generator for image sensors tests

Cryo-EM allows for the preservation of viability of biological samples, including infectious agents; therefore studying them in a microscope should be performed with proper precautions to protect research and maintenance personnel from infection by the samples studied. Since the microscope is installed in high biosafety containment, an adequate disinfection procedure should be implemented in the event of an incident or as a preventive measure prior to any maintenance requiring opening of the microscope column or vacuum system. We developed earlier ClO_2 decontamination protocols to disinfect the room, the microscope, ancillary equipment, and tools used in the containment.

Chlorine dioxide (ClO_2) is a strong oxidizer. It is used for decontamination in biological safety cabinets (isolators) [15,16], processing vessels [17], rooms [18], and large facilities [19]. It has to be used with >50% humidity to kill microbes [20,21,22] but could potentially damage equipment exposed to it.

Our JEM-2200FS has several digital cameras including a TVIPS FastScan-F114T CCD and a DE-20 direct detection camera. The cameras are not specifically designed to be used in BSL-3 containment. The image sensor module of the DE-20 and part of the control and readout electronics share vacuum with the microscope vacuum system and could therefore potentially be exposed to an infectious agent in case of an incident. In the case of the FastScan F114T, only its fiber optics assembly is exposed to the microscope vacuum. To test the durability of the sensors and camera

electronics inside the microscope vacuum system would require exposure of the lower part of the microscope column and would be disruptive for the operation of the microscope. We therefore used separate image sensors from the same type of cameras to analyze potential damage to the cameras from ClO_2 exposure. The testing was necessary since we have previously observed significant damage of a microscope fluorescent screen during preliminary decontamination tests of an electron microscope [2]. Our ClO_2 generator has a mixing chamber attached to it, which is large enough to accommodate small parts for off-line testing of ClO_2 exposure without involving the microscope in the gas flow loop.

We know from experience that electronic circuit boards can easily withstand multiple ClO_2 exposures, but the image sensors of CCD/CMOS cameras have not been thoroughly tested for potential damage by the gas. In the present experiment, we exposed image sensors (fiber optics plate coated with phosphor P43 (Gd_2O_2S:Tb) phosphor scintillator for the FastScan-F114T and the sensor module for Direct Electron cameras) to ClO_2 and ran special ClO_2 cycles to simulate several standard decontamination cycles in the microscope [2].

A phosphor scintillator for TVIPS FastScan-F114T was characterized at the factory in a FEI T12 electron microscope with its sensitivity to electrons and resolution measured before ClO_2 exposure. The scintillator was then sent to our facility and exposed in the mixing chamber. The total exposure (approx. 5 mg/L ClO_2, 1.6 hours) was equivalent to eight standard runs (1 mg/L ClO_2, 2 hours) used to decontaminate our microscope compartments. Immediately after purging the chamber with dry nitrogen, the scintillator was put into a vacuum coater (Cressington 308, Ted Pella, Inc., Redding, California, USA) and pumped overnight to remove residual ClO_2 from the scintillator surface. No visual damage was noted after the exposure (Figure 2A). The scintillator was sent back to TVIPS for further testing. The same measurements were repeated in the T12 electron microscope with the exposed scintillator. All measurements were done at 120 keV. Electron sensitivity before ClO_2 exposure was 21.5 counts/electron; after the exposure it became 20.5 counts/electron. The resolution was measured using NTF (noise transfer function) and line-scan across TEM beam stop [23,24]; before ClO_2 treatment it was 47.5% at ½ Nyquist frequency, 17.7% at Nyquist frequency, and after the exposure it changed to 45.0% at ½ Nyquist frequency, and to 18.1% at Nyquist frequency. Both, visual inspection and quantitative measurements of camera sensitivity and resolution confirmed that practically no damage was inflicted by ClO_2 exposure to the scintillator, meaning that the FastScan-F114T camera could be safely used in a BSL-3 containment with periodic decontamination cycles using ClO_2 gas. It was essential to use a scintillator assembly with an intact aluminum coating on top of the phosphor; scratches and holes in the coating would lead to damage of the phosphor, as was noticed with the fluorescent screen in the microscope [2].

A sensor module for a DE-12 camera was sent to UTMB after examination and characterization at the factory. The sensor was verified before to be functional, its dark and leakage current were measured as well as sensitivity to electrons at 200 keV, an edge profile and MTF (modulation transfer function). The module was then placed in the mixing chamber and exposed to ClO_2 in a similar way as was used with the TVIPS scintillator assembly, with the exposure equivalent to approximately ten standard ClO_2 cycles for microscope decontamination (6 mg/L ClO_2, 3.3 hrs). After purging the system with dry nitrogen to remove ClO_2 at the end of exposure the module was removed from the chamber and sent back to the factory in San Diego. Although we did not expect any long-term damage in our experiments based on our experience with the microscope decontamination, we decided to inspect for damage because of a previous report of long-term

damage to electronic components [25]. The sensor was kept in a dry clean place for at least a year. It was periodically inspected visually; no visible damage was observed on either the surface of the sensor or on the rest of the sensor module including solder joints, electronics, and the board itself (Figure 3). Minor contamination was noticed on bonding wires (Figure 3C) that could have resulted from residual ClO_2 gas not being completely removed by N_2 purging after the ClO_2 cycle. We did noticed damage in the microscope specimen chamber after an earlier decontamination run when no adequate ventilation of the exposed area was provided. After a year of observation the sensor was tested in a DE-12 camera; practically no performance change was noticeable based on sensitivity, edge profile, and MTF measurements (less than 5%). Therefore, Direct Electron sensors could also be safely used in a BSL-3 containment with periodic decontamination cycles using ClO_2 gas.

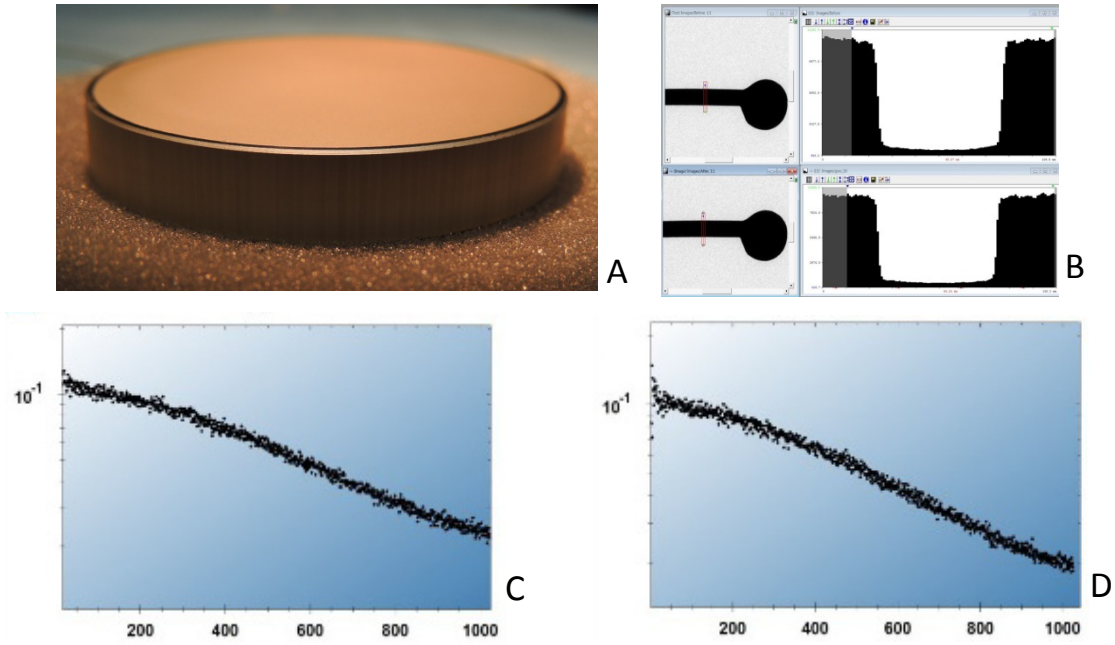

Figure 2 A. Overview of the TVIPS F114T scintillator surface after its exposure to ClO_2 equivalent to eight standard decontamination cycles of the microscope compartments. No visible damage was observed. B. Microscope beam stop images taken at 120 keV in FEI T12 before and after (upper and lower panels, accordingly) and corresponding linear profiles in right side of the panels. C. Noise Transfer Function (NTF) of the scintillator before ClO_2 exposure. D. Same but after ClO_2 treatment. No appreciable difference in the scintillator performance was measured.

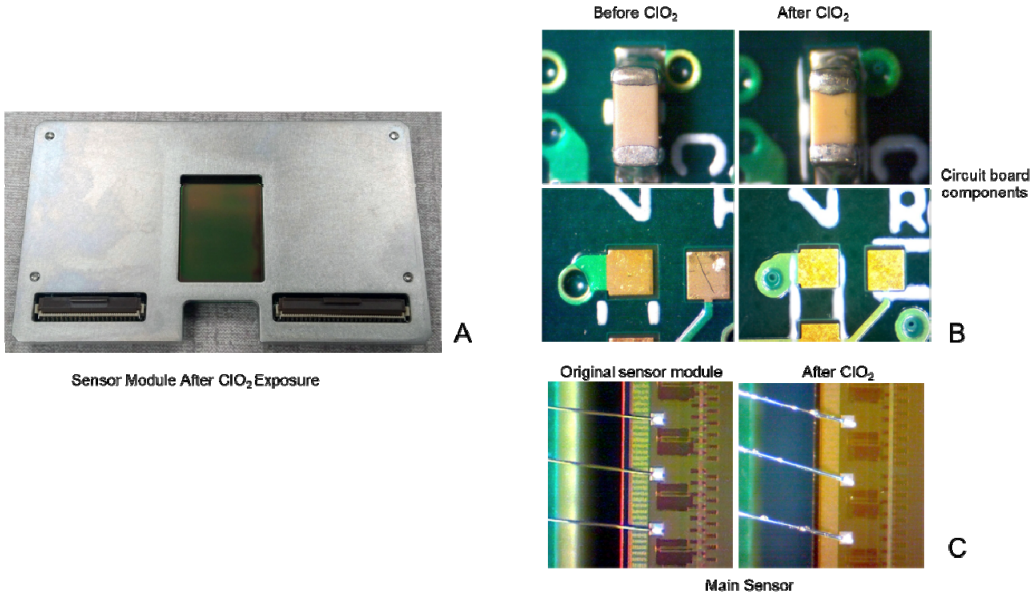

Figure 3. A. DE sensor module overview after ClO_2 treatment. No visible damage was detected. B. Electronics components on the sensor module board exposed to ClO_2. Left panels: before ClO_2 exposure, right ones: after ClO_2 treatment. No damage was visible. C. Bonding wires, before ClO_2 exposure (left) and after (right). Some contamination was visible on the wires that could be attributed to residual ClO_2 present after purging mixing chamber from ClO_2. In the real camera the sensor module would be pumped down to high vacuum immediately after the treatment eliminating that contamination.

3.2. TMV imaging in the microscope

Since our JEM-2200FS microscope was exposed to ClO_2 gas during previous decontamination cycles, we decided to image and reconstruct TMV to test the overall microscope performance. TMV is a well-characterized virus with robust helical structure [7,26–29], yielding high-resolution EM maps. It was therefore an ideal test specimen, since our results could be easily compared to previously published high-resolution reconstructions.

First, a small set of images was acquired to evaluate whether the microscope performed well enough to produce reasonable resolution images and to test the image processing workflow. Images were acquired using movie mode (continuous streaming at 25 frames per second delivering in-line dose fractionation); individual frames from each image were aligned and compensated for radiation damage with DE_process_frames.py script developed by Direct Electron. In the processed images, visible Thon rings extended to better than 6 Å. We used a combination of EMAN, EMAN2 and IMAGIC to pick helical segments of TMV, correct CTF, determine angular orientations, and calculate 3D reconstructions from the images. Segment picking and CTF correction was performed in EMAN (BOXER) and EMAN2 (CTFCOR). The rest of the processing was done in IMAGIC.

Even from that small set of images with only 630 segments, we were able to reconstruct a map with readily visible α-helices in the capsid protein, with the helical pitch resolved. Encouraged by that result we collected a larger data set and processed that in the same way. The resulting map was much

less noisy with clear helical pitch of the α-helices resolved. We then fitted the 2XEA.pdb structure in our reconstruction (Figure 4A), which demonstrated correlation of 73% with our map. We estimated the resolution of the two reconstructions with the Fourier Shell Correlation (FSC) function using the gold-standard criterion with two independently processed 3D reconstructions [13]). Using the 0.143 FSC criterion [30], the resolution of our map was approximately 6.3 Å (Figure 4B), demonstrating that the microscope was performing reasonably well even after potentially harsh treatment with a strong oxidizer like ClO_2.

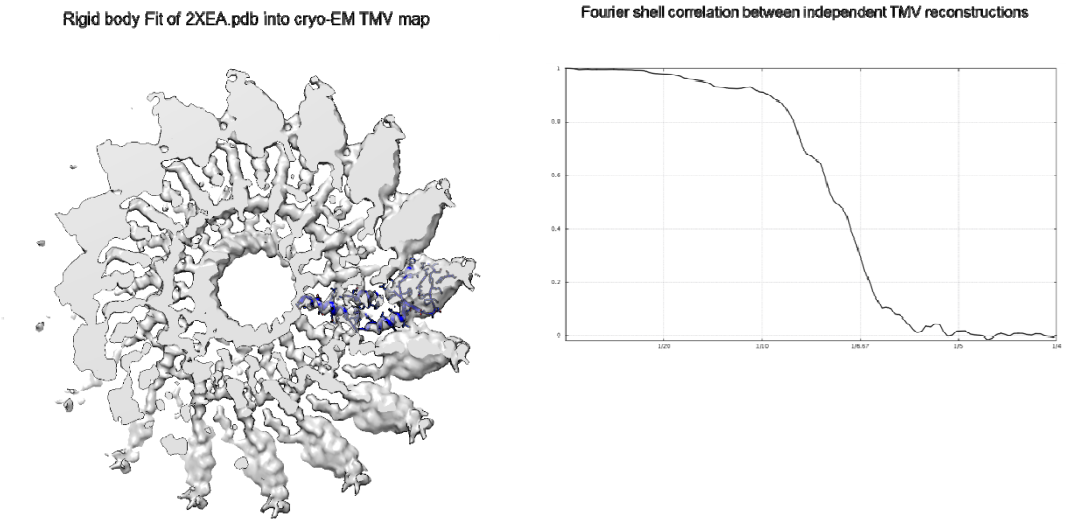

Figure 4. A. 6.3 Å resolution cryo-EM reconstruction of Tobacco Mosaic Virus (TMV). B. Fourier shell correlation (FSC) curve between two independently processed TMV data sets. According to the 0.143 "gold-standard" criterion, the resolution of the map on the left is approximately 6.3 Å.

4. Conclusion

In conclusion, our ClO_2 gas decontamination does not appear to significantly affect the performance or function of our TEM setup. We were able to achieve 6.3 Å resolution with the current state of the microscope. We demonstrated that CCD and CMOS electron detectors are safe to use in BSL-3 containments using ClO_2 gas for decontamination. In addition, our JEM-2200FS microscope performance remains at an acceptable level after repeated ClO_2 gas decontamination cycles.

Acknowledgments

Our TEM center was established through generous gifts from W. M. Keck Foundation, and the Kleberg Foundation, and by a grant from Health Resources and Services Administration. The center operation was supported in part by grants to MS and SCW from NIAID through the Western Regional Center of Excellence for Biodefense and Emerging Infectious Diseases Research, NIH grant number U54 AI057156. We are indebted to Dr. Bernard M. Pettitt for his support of the Center. The authors acknowledge scintillator and sensor testing by TVIPS and Direct Electron companies,

correspondingly.

Conflict of Interest

All Authors declare no conflicts of interest in this paper.

References

1. Sherman MB, Freiberg AN, Razmus D, et al. (2010) A Unique BSL-3 Cryo-Electron Microscopy Laboratory at UTMB. *Appl Biosaf* 15: 130–136.
2. Sherman MB, Trujillo J, Leahy I, et al. (2013) Construction and organization of a BSL-3 cryo-electron microscopy laboratory at UTMB. *J Struct Biol* 181: 223–233.
3. Sherman MB, Weaver SC (2010) Structure of the recombinant alphavirus Western equine encephalitis virus revealed by cryoelectron microscopy. *J Virol* 84: 9775–9782.
4. Wang Z, Hryc CF, Bammes B, et al. (2014) An atomic model of brome mosaic virus using direct electron detection and real-space optimization. *Nat Commun* 5: 4808.
5. Bammes B, Chen D, Jin L, et al. (2013) Visualizing and correcting dynamic specimen processes in TEM using a Direct Detection Device. *Microsc Microanal* 19: 1320–1321.
6. Clare DK, Orlova EV (2010) 4.6A Cryo-EM reconstruction of tobacco mosaic virus from images recorded at 300 keV on a 4k x 4k CCD camera. *J Struct Biol* 171: 303–308.
7. Fromm SA, Bharat TAM, Jakobi AJ, et al. (2015) Seeing tobacco mosaic virus through direct electron detectors. *J Struct Biol* 189: 87–97.
8. Ludtke SJ, Baldwin PR, Chiu W (1999) EMAN: semiautomated software for high-resolution single-particle reconstructions. *J Struct Biol* 128: 82–97.
9. Tang G, Peng L, Baldwin PR, et al. (2007) EMAN2: an extensible image processing suite for electron microscopy. *J Struct Biol* 157: 38–46.
10. van Heel M, Harauz G, Orlova EV, et al. (1996) A new generation of the IMAGIC image processing system. *J Struct Biol* 116: 17–24.
11. Namba K, Pattanayek R, Stubbs G (1989) Visualization of protein-nucleic acid interactions in a virus. Refined structure of intact tobacco mosaic virus at 2.9 A resolution by X-ray fiber diffraction. *J Mol Biol* 208: 307–325.
12. Holmes KC, Franklin RE (1958) The radial density distribution in some strains of tobacco mosaic virus. *Virology* 6: 328–336.
13. Henderson R, Sali A, Baker Matthew L, et al. (2012) Outcome of the First Electron Microscopy Validation Task Force Meeting. *Structure (London, England:1993)* 20–330: 205–214.
14. Pettersen EF, Goddard TD, Huang CC, et al. (2004) UCSF Chimera--a visualization system for exploratory research and analysis. *J Comput Chem* 25: 1605–1612.
15. Czarneski MA, Lorcheim P (2005) Isolator decontamination using chlorine dioxide gas. *Pharm Tech* 29: 124–133.
16. Eylath A, Wilson D, Thatcher D, et al. (2003) Successful sterilization using chlorine dioxide gas: Part one- Sanitizing an aseptic fill isolator. *BioProcess Int* 1: 52–56.
17. Eylath AS, Madhogarhia ER, P. L, et al. (2003) Successful sterilization using chlorine dioxide gas: Part two-Cleaning process vessels. *Bio-Process Int* 1: 54–56.
18. Leo F, Poisson P, Sinclair CS, et al. (2005) Design, development, and qualification of a

microbiological challenge facility to assess the effectiveness of BFS aseptic processing. *PDA J Pharm Sci Tech* 59: 33–48.
19. Czarneski MA (2009) Microbial decontamination of a 65- room new pharmaceutical research facility. *Appl Biosafety: J Amer Biolog Safety Association* 14 81–88.
20. Spotts Whitney EA, Beatty ME, Taylor TH, et al. (2003) Inactivation of Bacillus anthracis spores. *Emerg Infect Dis* 9: 623–627.
21. Agalloco J, Carleton P, Frederick J (2008) Validation of pharmaceutical processes. New York: Informa Healthcare USA Inc.
22. Westphal AJ, Price PB, Leighton TJ, et al. (2003) Kinetics of size changes of individual Bacillus thuringiensis spores in response to changes in relative humidity. *Proc Natl Acad Sci* 100: 3461–3466.
23. Meyer RR, Kirkland AI, Dunin-Borkowski RE, et al. (2000) Experimental characterisation of CCD cameras for HREM at 300 kV. *Ultramicroscopy* 85: 9–13.
24. Meyer RR, Kirkland AI (2000) Characterisation of the signal and noise transfer of CCD cameras for electron detection. *Microsc Res Tech* 49: 269–280.
25. Derkits GE, Mandich ML, Reents WD, et al. (2010) Reliability of electronic equipment exposed to chlorine dioxide used for biological decontamination. 879–880.
26. Namba K, Stubbs G (1986) Structure of TMV at 3.6 Å resolution: implications for assembly. *Science* 231: 1401–1406.
27. Champness JN, Bloomer AC, Bricogne G, et al. (1976) The structure of the protein disk of tobacco mosaic virus to 5A resolution. *Nature* 259: 20–24.
28. Sachse C, Chen JZ, Coureux PD, et al. (2007) High-resolution electron microscopy of helical specimens: a fresh look at tobacco mosaic virus. *J Mol Biol* 371: 812–835.
29. Ge P, Zhou ZH (2011) Hydrogen-bonding networks and RNA bases revealed by cryo electron microscopy suggest a triggering mechanism for calcium switches. *Proc Natl Acad Sci U S A* 108: 9637–9642.
30. Rosenthal PB, Henderson R (2003) Optimal determination of particle orientation, absolute hand, and contrast loss in single-particle electron cryomicroscopy. *J Mol Biol* 333: 721–745.

Disclosure Statement

JEOL is the manufacturer of the JEM-2200FS. Direct Electron is the manufacturer of the DE-12 and DE-20 cameras. TVIPS is the manufacturer of the FastScan-F114T camera.